Aerosol and Air Quality Research, 17: 923–935, 2017

ISSN: 1680-8584 print / 2071-1409 online
doi: 10.4209/aaqr.2016.05.0185

Technical Note

Analysis of the Temporal and Spatial Variation of Aerosols in the Beijing-Tianjin-Hebei Region with a 1 km AOD Product

Lin Sun[*], Rui-Bo Li[**], Xin-Peng Tian, Jing Wei

Geomatics College, Shandong University of Science and Technology, Shandong, Qingdao 266590, China

ABSTRACT

The Beijing-Tianjin-Hebei region is one of the most polluted areas in China, especially in terms of particulate matter pollution. To describe the aerosol distribution of such an area, the aerosol optical depth (AOD) with a 1 km spatial resolution was retrieved from MODIS data based on a new high-resolution <1000 m> aerosol retrieval algorithm with a priori land surface reflectance (LSR) database support (HARLS). Continuous AOD data from 2013 and 2014 retrieved by this algorithm were used to analyze the spatial and temporal distribution of the AOD in the above area. The AOD in the Beijing-Tianjin-Hebei region has obvious regional and seasonal variations. The AOD in the south and east is higher than in the north and west, and the AOD in spring and summer is higher than that in winter and autumn.

Keywords: AOD; High spatial resolution; Beijing-Tianjin-Hebei region; Temporal and spatial variation.

INTRODUCTION

With the rapid economic development of the Beijing-Tianjin-Hebei region, energy consumption has increased rapidly (Liu and Zhang, 2012), and air pollution has become an important environmental problem in this area. In recent years, haze weather, mainly caused by $PM_{2.5}$, occurs frequently (Zhao *et al*., 2013). Atmospheric particulate matter pollution in this region has become a focus issue for experts and the public (Wu, 2012; Bi *et al*., 2014; Che *et al*., 2015).

The current primary methods for the analysis of particles is via ground measurements (Holben *et al*., 1998, 2001), which have high accuracy but cannot comprehensively indicate the spatial distribution of particles because they are restricted by the distribution of detection sites. Remote sensing technology can effectively compensate for such a problem by utilizing continuous monitoring over a large-scale space. However, the main parameter of particles obtained by remote sensing technology is the aerosol optical depth (AOD), which is defined as the integrated extinction coefficient over a vertical column of unit cross section, expressing the subduction function of aerosols with light (Ångström, 1930; Van de Hulst, 1948). Research shows that the AOD retrieved by remote sensing technology, as the most basic optical property and major index of the environmental effects of aerosols, could indicate the content of particulate matter and atmospheric turbidity to some degree and therefore be used to describe the mass concentration distribution of atmospheric particles (Remer *et al*., 2005; Ramanathan *et al*., 2001; He *et al*., 2014).

Large-scale, real-time and dynamic detection of atmospheric particulates through remote sensing has become the major method for analyzing the temporal and spatial variation of particulates (Hutchison, 2003; Hutchison *et al*., 2004; De Meij *et al*., 2012; Zhang *et al*., 2012). With the rapid aggravation of particulate matter pollution in many areas of China recently, research on aerosol distributions over the whole country or in typical areas in China using remote sensing methods is gradually increasing. Luo *et al.* (2014) analyzed the AOD variation characteristics in China with MODIS AOD data from the most recent 10 years, revealing that the area of the Sichuan Basin is higher than other areas, followed by the Yangtze River, North China Plain and the Pearl River Delta. Using the comprehensive application of MODIS and MISR data and AERONET (Aerosol Robotic NETwork) ground measurements of the AOD, Qi *et al.* (2013) analyzed the aerosol distribution in China and found that the region of the Tarim Basin has the highest particulate matter distribution and the seasonal variation was not obvious. Using remote sensing technology to study the particulate pollution in typical areas in China has also been developed rapidly (Li *et al*., 2010; Zheng *et al*., 2011; Zheng *et al*., 2013; Ma *et al*., 2016; Bilal *et al.*, 2017). The Beijing-Tianjin-Hebei region is the most developed

[*] Corresponding author.
Tel.: +86-0532-88032922
E-mail address: sunlin6@126.com
[**] Corresponding author.
E-mail address: LRB0106@hotmail.com

region in northern China that contains many industries and a large population. This region has become one of the areas with the most severe air pollution in China because of the industrial development and concentrated population, seriously impacting the lives of the local people and the sustainable development of regional economies (Li *et al*., 2007; He *et al*., 2012). A clear understanding of the spatial and temporal distribution of particles in this area will aid the understanding of the cause of particulate pollution to guide prevention and remediation.

By analyzing the temporal and spatial characteristics of the particulate matter in the Beijing-Tianjin-Hebei-Shanxi-Shandong region from MODIS aerosol products obtained in 2000–2013, Liu *et al.* (2015) divided the period of particulate matter pollution into two phases: an obvious increasing period during 2000–2007 and an apparent decreasing period during 2008–2013. Studies have been conducted to determine the aerosol distribution in the Beijing-Tianjin-Hebei region. However, the AODs used in these works were general and with low spatial resolution because the current AOD retrieval algorithm can obtain the AOD in high precision only in areas with water and dense dark vegetation coverage. For urban and arid regions, it is not easy to obtain high-precision AOD products (Hsu *et al.*, 2013). Limited by the current AOD retrieval algorithm, the AOD product used for particle analysis has a low spatial resolution and spatial discontinuity, for example, the spatial resolution of MOD04, produced by NASA, is 10 km × 10 km and 3 km × 3 km (Levy *et al.*, 2009; Huang *et al*., 2010; Jiang *et al*., 2013), which cannot describe the particle distribution in detail.

To obtain AOD data with high resolution and spatial continuity, Sun *et al*. (2015) proposed an AOD retrieval algorithm supported by prior land surface reflectance data to retrieve the AOD from the Landsat 8 OLI; this algorithm was then updated by Wei and Sun (2016) to inverse the AOD with a high resolution of 1 km from MODIS data. A land surface reflectance database was built based on a high-quality MODIS land surface reflectance product (MOD09A1) and was applied to propose the land surface reflectance to support aerosol retrieval from MODIS data (HARLS). To obtain a new HARLS algorithm for estimating the land surface reflectance (Sun *et al*., 2015; Sun *et al*., 2016), this algorithm completes the AOD retrieval with high precision over areas for which the dark target algorithm is not available (Sun *et al.*, 2010). The resolution of AOD products obtained through this algorithm is 1 km. This algorithm was used to realize AOD retrieval during 2013–2014 in the Beijing-Tianjin-Hebei region.

DATA AND METHOD

Data Resources and Aerosol Retrieval

A total of 714 MODIS L1B images with less clouds in 2013 and 2014 were selected to analyze the AOD distribution of the Beijing-Tianjin-Hebei region (Fig. 1). MODIS was launched by the EOS Terra/AM satellite in 1999 and by the Aqua/PM satellite in 2002 (Salomonson *et al*., 1989; King *et al*., 1992). This sensor obtains data from 36 spectral bands, covering the visible to infrared wavelengths, and provides earth surface observation data every 1–2 days. MODIS is

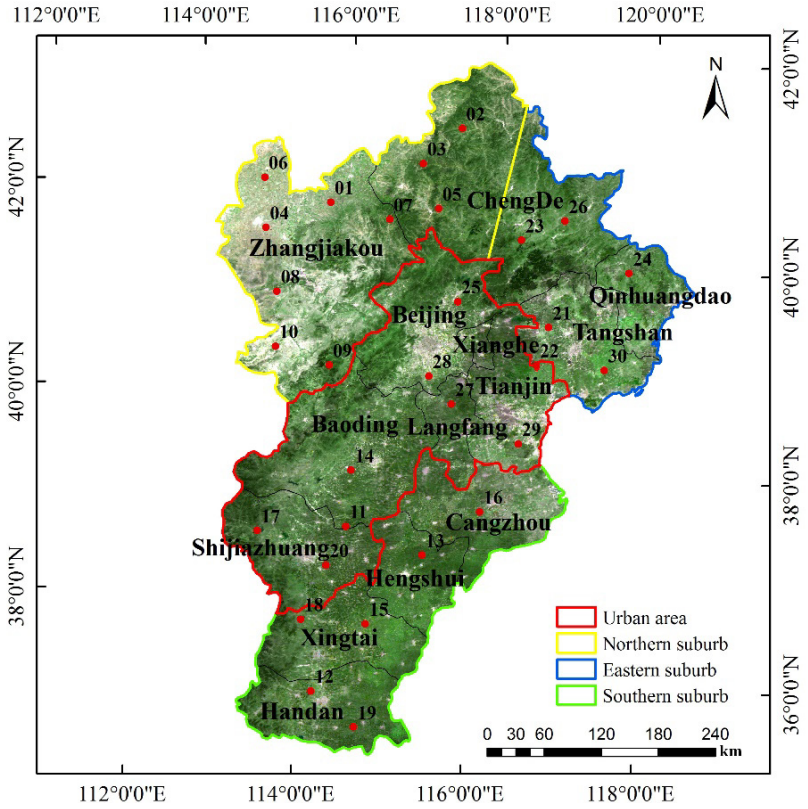

Fig. 1. True color image of the Beijing-Tianjin-Hebei region.

mainly used to observe solar radiation, as well as the atmosphere, oceans and land, for long-term monitoring and research on the environmental variation of the atmosphere and earth. With wide band coverage, moderate spatial resolution and a short revisiting period, this sensor is widely used in aerosol remote sensing monitoring.

In areas with low surface reflectance, satellite-measured reflectance obviously increases with the increase in the AOD (Kaufman and Sendra, 1988; Kaufman *et al*., 1997), and satellite signals can obviously identify AOD variations, which could realize a highly accurate AOD retrieval. Water has low surface reflectance in the visible and near-infrared bands, and dense vegetation also has low surface reflectance in the red (0.6–0.7 μm) and blue (0.4–0.5 μm) bands; therefore, such areas are suitable for AOD retrieval (Kaufman and Sendra, 1988). King *et al*. (1999) conducted a highly accurate AOD retrieval over land; the surface reflectance accuracy should be controlled at 0.005–0.01, which could lead to an AOD error of 0.05–0.10. For most water areas, the surface reflectance accuracy determined by empirical methods could reach this criterion. The determination method for dense vegetation reflectance has been improved to increase the retrieval accuracy in recent years. For sparse vegetation and urban areas, higher surface reflectance accuracy is required because aerosols are more difficult to identify from satellite signals. However, the surface reflectance in such areas is difficult to determine due to the complex components, and the aerosol retrieval in such areas is therefore greatly limited (Li *et al*., 2013).

Sun *et al.* (2016) proposed an AOD remote sensing retrieval algorithm (HARLS) to solve the aerosol retrieval in areas not covered by dense vegetation. In this algorithm, the highly accurate surface reflectance of retrieval images is determined from high-quality surface reflectance products obtained from MODIS land surface reflectance (MOD09) products to realize AOD retrieval from the Landsat 8 OLI in areas with sparse vegetation coverage or urban areas. A surface reflectance database was built from 8 days of MOD09A1 data with a spatial resolution of 500 m. To reduce the influence of cloud pixels, a monthly surface reflectance database was produced from MOD09A1 data using the method of minimum data synthesis. The influence of surface coverage and phenological changes were also considered when the land surface reflectance was estimated for the AOD retrieval data. Based on this, Wei and Sun (2016) updated this algorithm and applied it to AOD retrieval with 1 km resolution in the Beijing-Tianjin-Hebei region from MODIS data.

Different from the algorithms used for dense vegetation-covered areas that utilize short-wave infrared bands to estimate the land surface reflectance for AOD retrieval, this algorithm uses the prior land surface reflectance obtained from satellite data via atmospheric correction. Such an algorithm can effectively reduce the land surface reflectance error caused by a complex land surface structure, especially for areas with urban and sparse vegetation coverage, which are the main land types in the Beijing-Tianjin-Hebei region. The MOD09 data used as the prior land surface reflectance was verified to have high precision (Vermote and Vermeulen, 1999; Vermote and Kotchenova, 2008), and such data can provide the land surface reflectance at several observation angles in a short period time with a high revisit frequency, which can reduce the effect of directional reflection on the retrieval accuracy. Another advantage of using MOD09 to support AOD retrieval from MODIS data is the lack of influence of spectral differences because these data originate from the same sensor. Such method has been used in previous studies for aerosol retrieval over different areas (Bilal *et al.*, 2013, 2014; Bilal and Nichol, 2015).

Figs. 2 and 3 show the retrieval results for the DT, DB and HARLS algorithms, in which Figs. 2(a), 3(a), 2(b) and 3(b) show the retrieval results from MOD04 (C6) by the DT and DB algorithms at 550 nm with a spatial resolution of 10 km and Figs. 2(c) and 3(c) show results for the HARLS algorithm with a spatial resolution of 1 km. Although retrieved by different algorithms, the retrieval results have the same trend, following a decreasing tendency from the center to the margin on the same day. However, the area retrieved by the DT algorithm was much less than those retrieved by the DB and HARLS algorithms. Fig. 1 illustrates that the areas retrieved by the DT algorithm are mostly vegetation-covered areas. Meanwhile, the DB algorithm is restricted to retrieval over urban areas with high surface reflectance, which also impacts the temporal continuity. The HARLS algorithm can obtain continuous AOD values over urban areas with high surface reflectance and complex surface structures; moreover, the retrieval results are obviously better than the MOD04 products owing to higher spatial resolution.

Verification and Analysis

AERONET, a federation of ground-based remote sensing aerosol networks established by NASA and PHOTONS (Holben *et al*, 1998; Holben *et al*, 2001), is the principle validation data used in verifying aerosol retrieval results. AOD data are computed at 3 data quality levels for 7 wavebands at approximately 800 sites globally, and the retrieval results are 3–5 times more accurate than those from satellites (Remer, 2009). Level 2.0 aerosol products with cloud exclusion and quality control are most widely used in the verification of aerosol retrieval (Smirnov *et al*, 2000).

To verify the retrieval accuracy of the model, the Level 2.0 products of 4 AERONET sites over the Beijing-Tianjin-Hebei area were applied (Fig. 1). The AOD at 550 nm is excluded, and the AOD data acquisition time is not identical to the time spent passing over a territory. Moreover, the spatial scale of the AERONET data differs from that of the satellite data, and the AODs were processed in order to maintain spectral, spatial and temporal consistency.

Based on the Ångström formula (Ångström, 1964) and AOD interpolation of AERONET data at 440 nm and 870 nm, the AOD at 550 nm can be derived (Eq. (1)).

$$\tau_\alpha(\lambda) = \beta\lambda^{-\alpha} \tag{1}$$

where $\tau_\alpha(\lambda)$ is the AOD at wavelength λ and α and β are the Ångström exponent and atmospheric turbidity coefficient, respectively, related to the total aerosol particle number, particulate size distribution and complex refraction index.

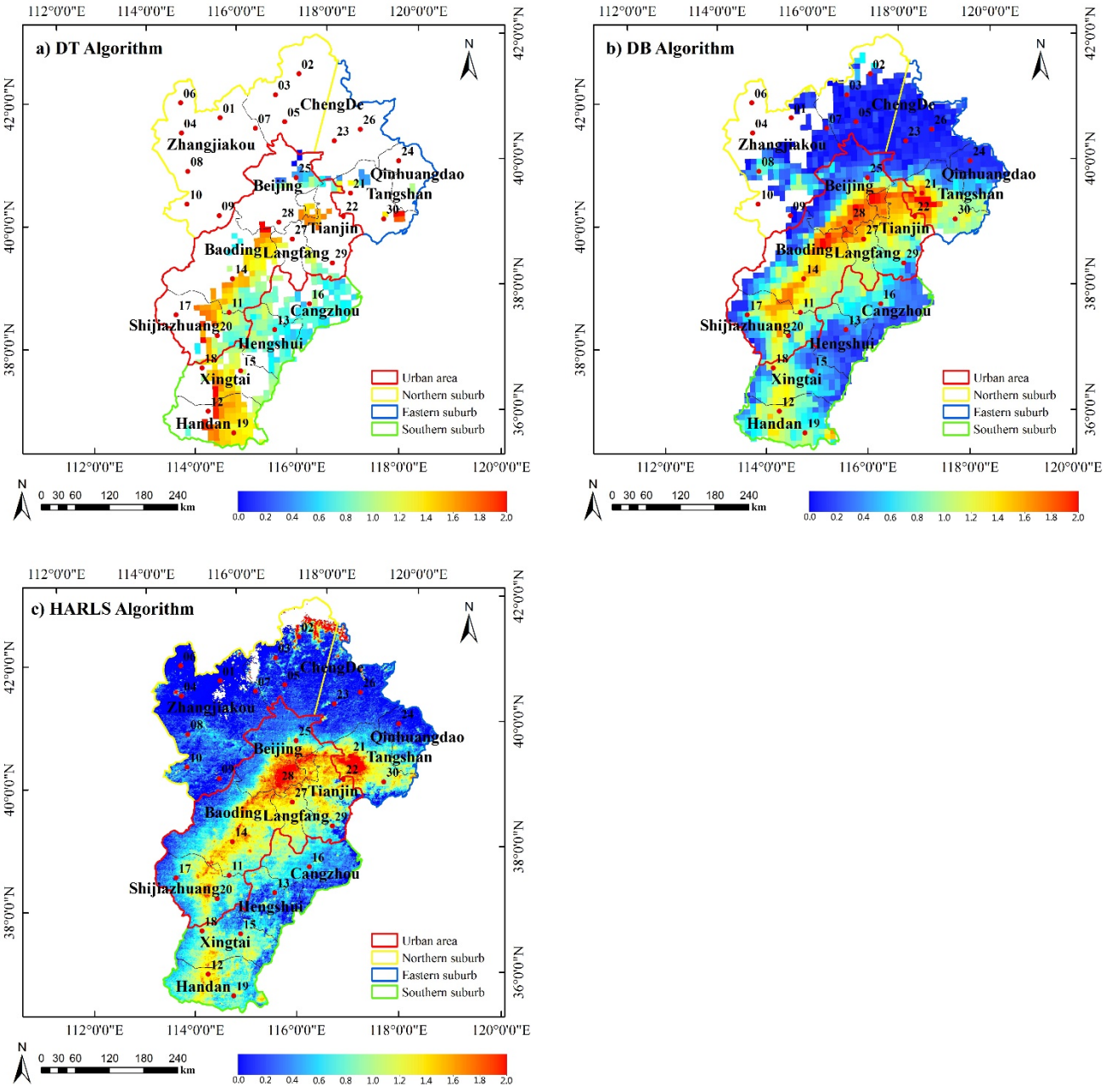

Fig. 2. Distribution of the aerosol optical thickness at 550 nm on April 2, 2013.

On a temporal scale, we consider that the aerosol variation within a short period of time is linear. The AERONET measured values of two moments that are closest to the imaging time were applied to calculate the AOD of the corresponding time by linear interpolation (Eq. (2)) (Benas *et al.*, 2013; Sun *et al.*, 2016):

$$\tau = \tau_1 \frac{t_2 - t}{t_2 - t_1} + \tau_2 \frac{t - t_1}{t_2 - t_1} \tag{2}$$

where τ is the AOD at the imaging time of the satellite images, t is the imaging time, t_1 and t_2 are the two moments closest to the imaging time, and τ_1 and τ_2 are the AODs at the imaging time.

On a temporal scale, in order to decrease the impact of unstable atmospheric factors, such as thin clouds, broken clouds and cloud edges, on the retrieval results, we applied 3 × 3 sample scales to the HARLS retrieval results with a 1 km resolution. After excluding abnormal AODs, the average value was taken as the retrieval value. The MOD04 (C6) aerosol products at 550 nm were compared with the DT and DB algorithms. Because of the low spatial resolution, a point-to-point sampling method was used; if there is no effective value, those in the 3 × 3 spatial scale are accepted. The correlation coefficient (R), root-mean-square error (RMSE) and expected error (EE) line were adopted as accuracy verification standards (Eqs. (3)–(5)):

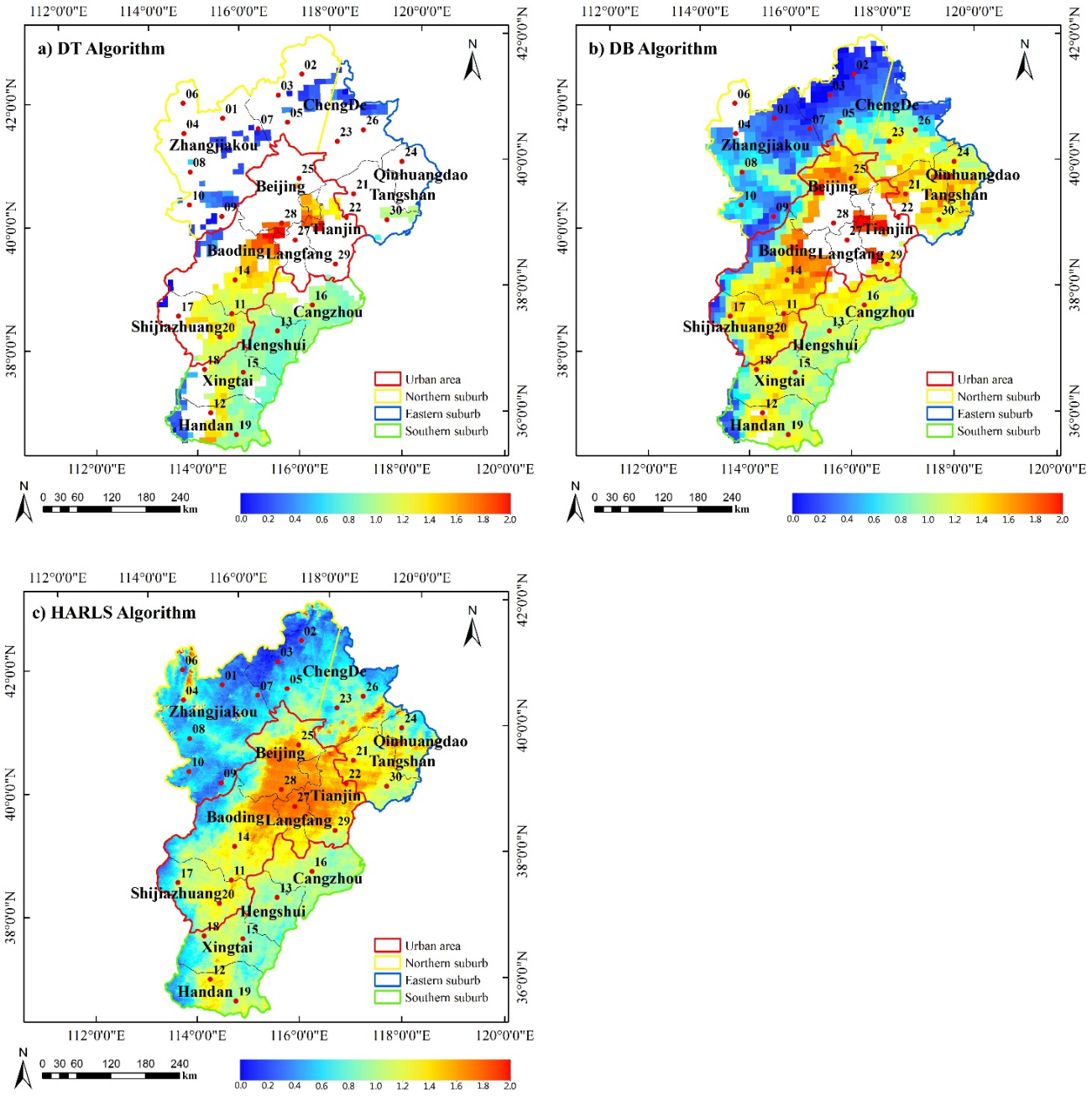

Fig. 3. Distribution of the aerosol optical thickness at 550 nm on April 8, 2014.

$$R = \frac{\sum_{i=1}^{n}(x_i - \bar{x})(y_i - \bar{y})}{\sqrt{\sum_{i=1}^{n}(x_i - \bar{x})^2 \times \sum_{i=1}^{n}(y_i - \bar{y})^2}} \quad (3)$$

$$RMSE = \sqrt{\frac{1}{n}\sum_{i=1}^{n}(x_i - y_i)^2} \quad (4)$$

$$EE = \pm(0.05 + 0.2x_i) \quad (5)$$

where x_i is the measured AOD at the AERONET site, y_i is the retrieval AOD, and $\bar{x}$ and $\bar{y}$ are the average values. The EE is the MOD04 verification standard (Eq. (6)) (Ichoku *et al.*, 2004):

$$\Delta\tau_\alpha = \pm 0.05 \pm 0.2\tau_\alpha \quad (6)$$

where τ_α is the AOD.

As is indicated in Table 1, N is the number of effective values verified by the DT, DB and HARLS algorithms. The value of the correlation coefficient (R) is (–1, 1), showing the degree of correlation. R > 0 indicates positive correlation, and R < 0 indicates negative correlation. The closer that R is to 1, the better the positive correlation. The R of the HARLS

Table 1. Evaluation Statistics for the MOD04 C6 DT, C6 DB (10 km), and New (1 km) Algorithm Retrievals with Respect to the AERONET AOD.

(a) Beijing

	C6 DT	C6 DB	HARLS
N	200	357	262
R	0.896	0.8887	0.8962
RMSE	0.328	0.328	0.131
= EE %	38.5	56.3	63.36
> EE %	59.5	36.97	18.32
< EE %	2	6.72	18.32

(b) Beijing_CAMS

	C6 DT	C6 DB	HARLS
N	158	291	202
R	0.8799	0.8488	0.9186
RMSE	0.339	0.419	0.132
= EE %	34.81	45.7	64.36
> EE %	63.92	48.8	21.29
< EE %	0.27	5.5	14.36

(c) Beijing_RADI

	C6 DT	C6 DB	HARLS
N	195	375	174
R	0.9067	0.894	0.9218
RMSE	0.275	0.37	0.119
= EE %	45.13	54.93	66.09
> EE %	54.36	40.27	16.09
< EE %	0.51	4.8	17.82

(d) XiangHe

	C6 DT	C6 DB	HARLS
N	253	372	280
R	0.9619	0.9199	0.9453
RMSE	0.223	0.308	0.12
= EE %	63.24	58.6	68.57
> EE %	35.97	33.06	19.64
< EE %	0.79	8.33	11.79

algorithm is above 0.9, higher than those of the DT and DB algorithms. The RMSE indicates the accuracy: the smaller the RMSE, the higher the accuracy. The RMSE of HARLS is approximately 0.1, but the RMSEs of the DT and DB algorithms range from 0.2–0.4, which are obviously higher than that of the HARLS algorithm. More than 60% of the results of the HARLS algorithm are within the EE (= EE), and the proportions of overrating (> EE) or underrating (< EE) are roughly equal. However, the DT and DB algorithms show obvious overrating. This analysis indicates that the HARLS algorithm is more accurate in retrieving the AOD, which has also better spatial continuity than MODIS products (Wei and Sun, 2016).

ANALYSIS OF THE TEMPORAL AND SPATIAL VARIATION OF THE AOD

Analysis of the Temporal Distribution

To study the total AOD variation in the Beijing-Tianjin-Hebei region, the area was divided into four parts according to economic development and population distribution: one central urban area (Beijing, Baoding, Shijiazhuang, Tianjin and Langfang) and three suburban areas (a northern suburb including western Chengde and Zhangjiakou; an eastern suburb including eastern Chengde, Qinhuangdao and Tangshan; and a southern suburb including Handan, Xingtai, Hengshui and Cangzhou). The average AOD of 30 detection sites with a 5 × 5 sample space were selected randomly to analyze the AOD variation in 2013 and 2014. Furthermore, March to May are taken as spring, June to August as summer, September to November as autumn and December to the next February as winter for a quarterly analysis (Liu *et al*., 2014).

Figs. 4 and 5 show the AOD variation of the Beijing-Tianjin-Hebei region in 2013 and 2014, for which the monthly data from each detection site was accumulated as daily data, covering 4065 pairs of data in 2013 and 3889 pairs of data in 2014. The monthly AOD is primarily between 0.1–1.5; a high AOD persists from February to June and a low AOD persists from September to the next January. In addition, a low AOD presents a downward trend after first increasing. In other words, the AOD variation in this area is higher in spring and summer and lower in autumn and winter.

This paper applied 8 detection sites that have the most effective value to analyze the seasonal variation of the AOD in 2013 and 2014, taking the data of 2014 as an example. Fig. 6 indicates that the AOD changes more frequently in spring and summer.

The AOD variation is more frequent in spring, with an obvious variation trend. In spring, burning straw to fatten farmland increases the AOD in some areas. Moreover, sand dust weather occurs frequently in spring, suspending dust particulates in the air, increasing the AOD (Li *et al*., 2010; Wang *et al*., 2015b).

In summer, the high AOD is higher overall but infrequent. From June to September, the Beijing-Tianjin-Hebei region experiences a major flooding period with higher temperature and humidity. According to a previous study, aerosol particulates with adsorbed moisture can affect the atmosphere as condensation nuclei, increasing the amount and concentration of cloud droplets, which increase the cloud optical depth (Twomey and Squires, 1959).

In autumn and winter, the high AOD decreases gradually, and the AOD of the central urban area exhibits rapid fluctuation. Snowfall and rainfall could eliminate aerosol particulates through wet deposition. Furthermore, the winter monsoon from Siberia and Mongolia promotes the transportation and scattering of aerosols. However, heating contributes greatly to aerosol emissions, resulting in the appearance of several aerosol peaks in this season (Zhao *et al*., 2013).

Analysis of the Spatial Distribution

As shown in Figs. 4 and 5, the AOD decreases from the southern suburb to the northern suburb, which covers central urban and eastern suburban areas. The northern suburban

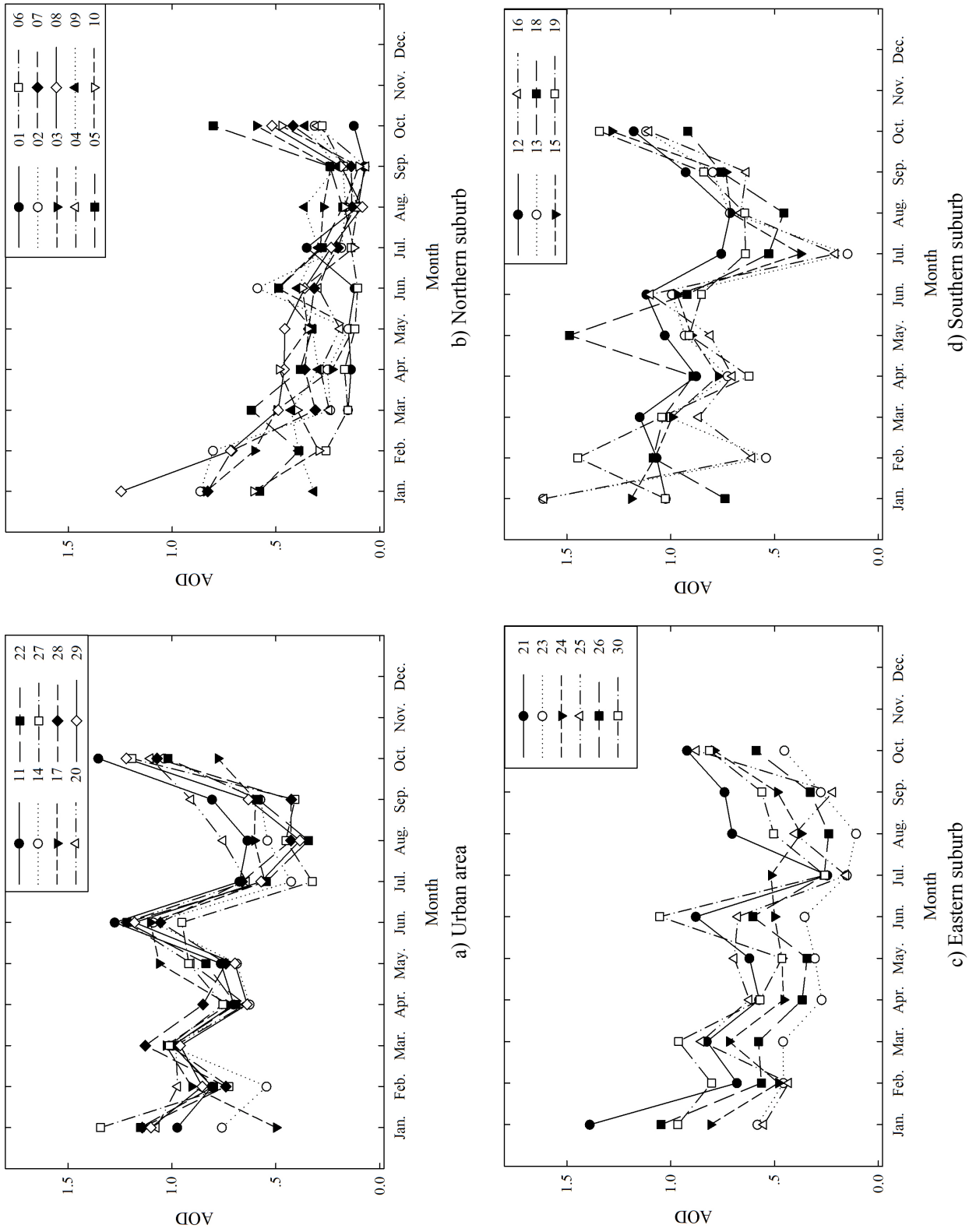

Fig. 4. AOD variation of the Beijing-Tianjin-Hebei region in 2013.

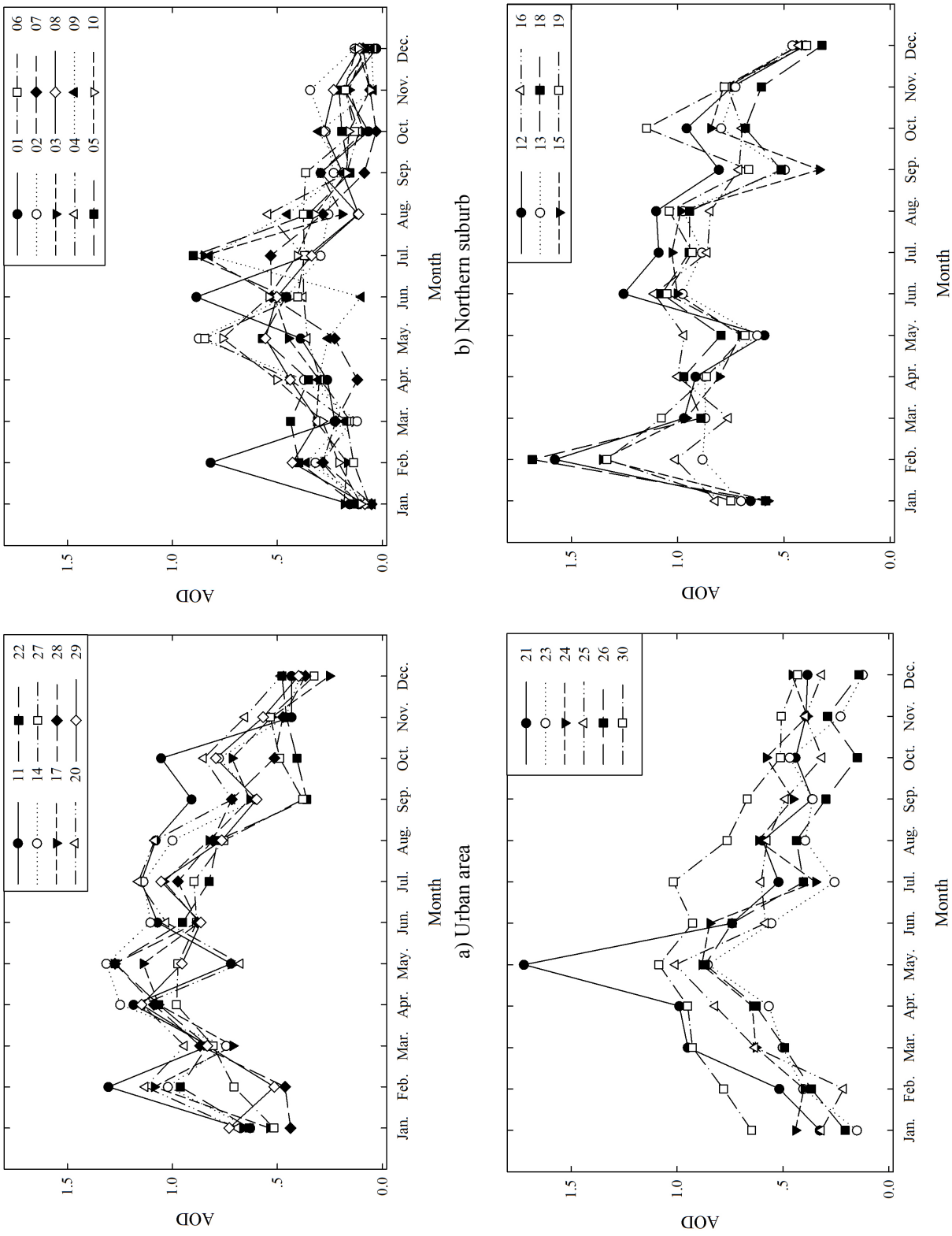

Fig. 5. AOD variation of the Beijing-Tianjin-Hebei region in 2014.

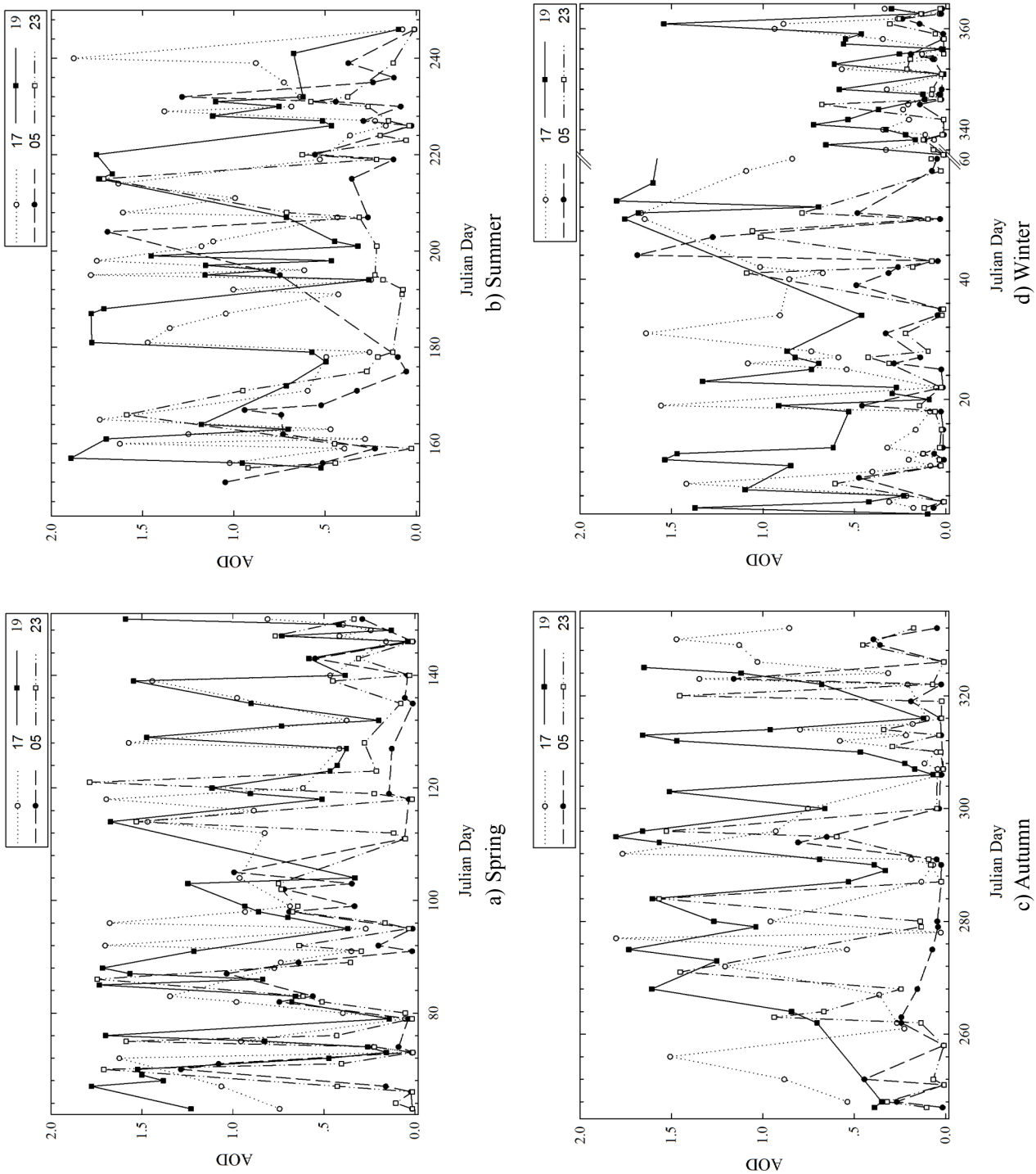

Fig. 6. Seasonal AOD variation of the Beijing-Tianjin-Hebei region in 2014.

area has the lowest AOD, which is lower than 1.0. The AOD variation in the southern suburb is the most unstable and is higher than 1.0 in several months. Moreover, the AOD variation for the central urban area is relatively stable with an overall higher AOD. In conclusion, the AOD in urban areas centered in Beijing, Tianjin, and Shijiazhuang increases to the south and east and decreases to the north, which is also shown in Fig. 7 (Wang *et al*., 2015a).

The seasonal distribution of the AOD for the Beijing-Tianjin-Hebei region in 2014 was acquired from the accumulated average daily data to analyze the spatial distribution of the AOD in 2014. The retrieval results show that the AOD is higher for the eastern and southern Beijing-Tianjin-Hebei region. As shown in Fig. 7(a), spring had the highest AOD, which was higher than 1.6 in eastern area of Tianjin and Langfang. According to Fig. 7(b), the higher AOD transferred to the western area, outspreading to Zhangjiakou and Chengde. From Fig. 7(c), the AOD decreased rapidly in autumn, and higher values concentrated in the southern area. Fig. 7(d) indicates that the AOD variation was stable in winter with a relatively mean distribution. Overall, the AOD was higher in the eastern and southern Taihang Mountains and Yanshan Mountains.

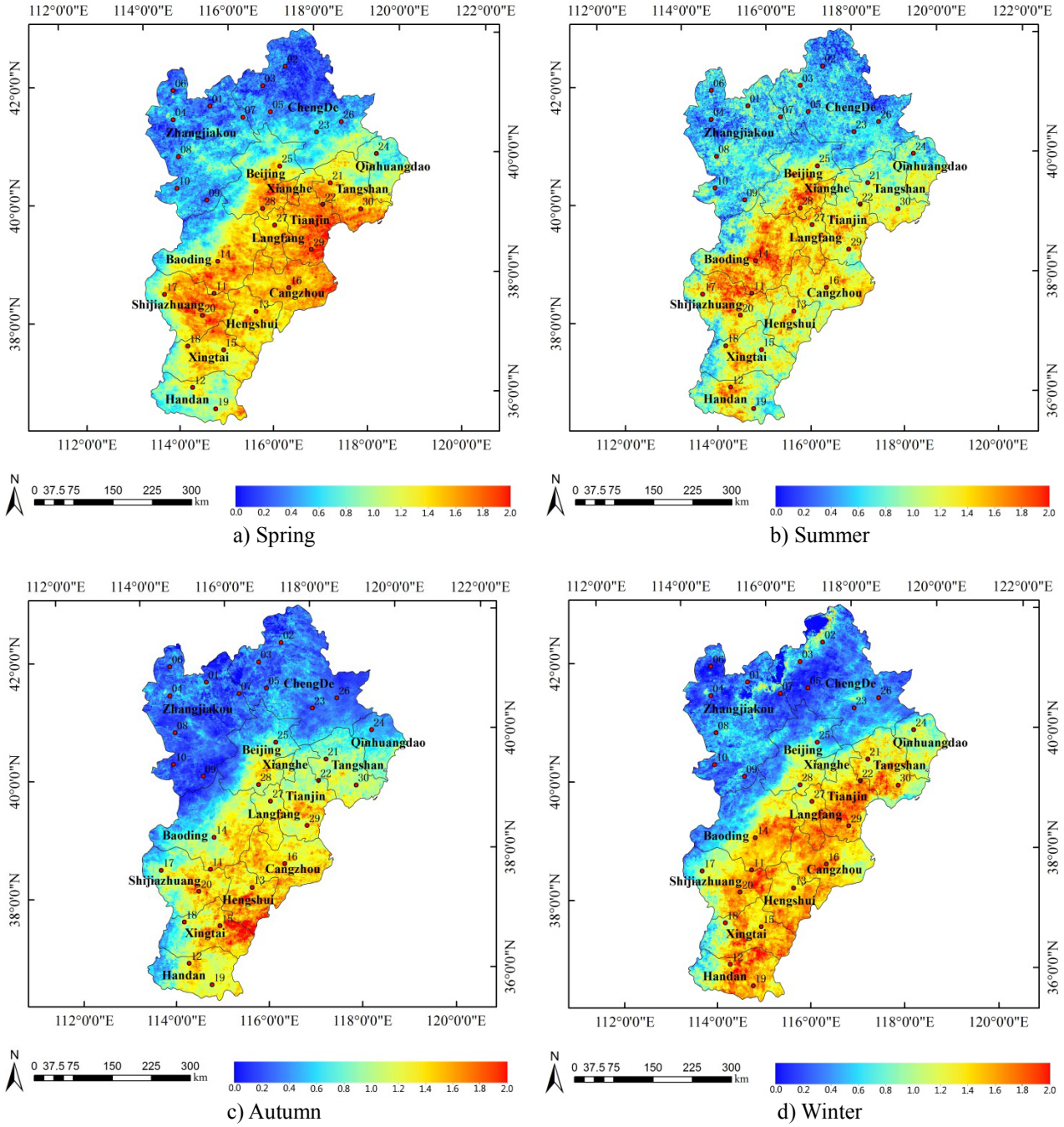

Fig. 7. Spatial distribution of the seasonal AOD variation of the Beijing-Tianjin-Hebei region in 2014.

CONCLUSION AND DISCUSSION

Based on MODIS L1B data from 2013–2014, the AOD for the Beijing-Tianjin-Hebei area with high spatial resolution was retrieved, and the spatial and temporal variation of the AOD over the Beijing-Tianjin-Hebei region was analyzed on the basis of the retrieved AOD. The conclusions are as follows:

1) The HARLS algorithm can be applied to urban areas with higher surface reflectance and complex surface structures to derive continuous AOD values with high spatial resolution, which conventional aerosol retrieval algorithms are unable to accomplish.
2) The AOD variation of Beijing-Tianjin-Hebei is regional and is greatly affected by landform and climate. Higher AODs concentrate in the eastern and southern Taihang Mountains and Yanshan Mountains, where the monsoon increases the AOD in hills and plains.
3) The seasonal variation of the AOD is obvious. The AOD in spring and summer is higher than that in winter and autumn; in addition, the range and frequency of the higher value is more apparent in spring and summer than in autumn and winter.
4) The spatial distribution of the AOD decreased from southern suburbs to northern suburbs, covering central urban and eastern suburban areas, and increased gradually from the central urban areas to the southern and eastern areas.
5) The area centered on Beijing, Tianjin and Shijiazhuang has rapid industrial development and a large population, resulting in a higher AOD, which also indicates that human activities such as vehicle exhaust emissions and industrial combustion are a primary source of aerosols.

This paper verified AOD retrieval and studied the spatial and temporal variation of the AOD in the Beijing-Tianjin-Hebei region, combined with the variation due to the landform, climate and human activity. However, changes in the stability of the AOD were affected by several factors. Therefore, subsequent studies should consider focusing on the relationships between the spatial and temporal variation of the AOD and influencing factors.

ACKNOWLEDGMENTS

The authors thank the Goddard Space Flight Center (GSFC) (http://ladsweb.nascom.nasa.gov) for providing the MODIS data and Dr. H.-B. Chen, Dr. P. Goloub, etc., for their effort in processing the AOD from AERONET used in this paper. The authors also thank the Graduate Innovation Fund of Shandong University of Science and Technology [SDKDYC170103], the National Natural Science Foundation of China [41171270] and the Outstanding Youth Foundation of Shandong Province [JQ201211].

REFERENCES

Ångström, A. (1930). On the atmospheric transmission of sun radiation II. *Geografiskaannaler* 12: 130–159.

Ångström, A. (1964). The parameters of atmospheric turbidity. *Tellus* 16: 64–75.

Benas, N., Chrysoulakis, N. and Giannakopoulou, G. (2013). Validation of MERIS/AATSR synergy algorithm for aerosol retrieval against globally distributed AERONET observations and comparison with MODIS aerosol product. *Atmos. Res.* 132–133: 102–113.

Bi, J., Huang, J., Hu, Z., Holben, B.N. and Guo, Z. (2014). Investigating the aerosol optical and radiative characteristics of heavy haze episodes in Beijing during January of 2013. *J. Geophys. Res.* 119: 9884–9900.

Bilal, M., Nichol, J.E. and Chan, P.W. (2014). Validation and accuracy assessment of a Simplified Aerosol Retrieval Algorithm (SARA) over Beijing under low and high aerosol loadings and dust storms. *Remote Sens. Environ.* 153: 50–60.

Bilal, M. and Nichol, J.E. (2015). Evaluation of MODIS aerosol retrieval algorithms over the Beijing-Tianjin-Hebei region during low to very high pollution events. *J. Geophys. Res.* 120: 7941–7957.

Bilal, M., Nichol, J.E. and Spak, S.N. (2017). A new approach for estimation of fine particulate concentrations using satellite aerosol optical depth and binning of meteorological variables. *Aerosol Air Qual. Res., in Press.*

Bilal, M., Nichol, J.E., Bleiweiss, M.P. and Dubois, D. (2013). A Simplified high resolution MODIS Aerosol Retrieval Algorithm (SARA) for use over mixed surfaces. *Remote Sens. Environ.* 136: 135–145.

Che, H., Xia, X., Zhu, J., Wang, H., Wang, Y., Sun, J., Zhang, X. and Shi, G. (2015). Aerosol optical properties under the condition of heavy haze over an urban site of Beijing, China. *Environ. Sci. Pollut. Res. Int.* 22: 1043–1053.

De Meij, A., Pozzer, A. and Lelieveld, J. (2012). Trend analysis in aerosol optical depths and pollutant emission estimates between 2000 and 2009. *Atmos. Environ.* 51: 75–85.

He, J., Zha, Y., Zhang, J. and Gao, J. (2014). Aerosol indices derived from Modis data for indicating aerosol-induced air pollution. *Remote Sens.* 6: 1587–1604.

He, Q., Li, C., Geng, F., Lei, Y. and Li, Y. (2012). Study on long-term aerosol distribution over the land of East China using MODIS data. *Aerosol Air Qual. Res.* 12: 304–319.

Holben, B.N., Eck, T.F., Slutsker, I., Tanré, D., Buis, J.P., Setzer, A., Vermote, E., Reagan, J.A., Kaufman, Y.J., Nakajima, T. and Lavenu, F., Jankowiak, I. and Smirnov, A. (1998). AERONET-A federated instrument network and data archive for aerosol characterization. *Remote Sens. Environ.* 66: 1–16.

Holben, B.N., Tanré, D., Smirnov, A., Eck, T.F., Slutsker, I., Abuhassan, N., Newcomb, W.W., Schafer, J.S., Chatenet, B., Lavenu, F. and Kaufman, Y.J., Castle, J.V., Setzer, A., Markham, B., Clark, D., Frouin, R., Halthore, R., Karneli, A., O'Neill, N.T. and Pietras, C. (2001). An emerging ground-based aerosol climatology: Aerosol optical depth from AERONET. *J. Geophys. Res.* 106: 12067–12097.

Hsu, N.C., Jeong, M.J., Bettenhausen, C., Sayer, A.M., Hansell, R., Seftor, C.S., Huang, J. and Tsay, S.C. (2013).

Enhanced deep blue aerosol retrieval algorithm: The second generation.*J. Geophys. Res.* 118: 9296–9315.

Huang, J., Li, F., Deng, X.J., Bi, X.Y. and Tan, H.B. (2010). Evaluation of the MODIS aerosol depth product over urban areas of the Pearl River Delta. *J. Trop. Meteorol.* 26: 526–532.

Hutchison, K.D. (2003). Applications of MODIS satellite data and products for monitoring air quality in the state of Texas. *Atmos. Environ.* 37: 2403–2412.

Hutchison, K.D., Smith, S. and Faruqui, S. (2004). The use of MODIS data and aerosol products for air quality prediction. *Atmos. Environ.* 38: 5057–5070.

Ichoku, C., Kaufman, Y.J., Remer, L.A. and Levy, R. (2004). Global aerosol remote sensing from MODIS. *Adv. Space Res.* 34: 820–827.

Jiang, Z., Chen, L.F., Wang, Z.T. and Tao, M.H. (2013). The analysis of spatiotemporal variation characteristics of tropospheric aerosol over the Pearl River Delta. *Chin. J. Geophys.* 56: 1835–1842 (in Chinese).

Kaufman, Y.J. and Sendra, C. (1988). Algorithm for automatic atmospheric corrections to visible and near-IR satellite imagery. *Int. J. Remote Sens.* 9: 1357–1381.

Kaufman, Y.J., Tanré, D., Remer, L.A., Vermote, E.F., Chu, A. and Holben, B.N. (1997). Operational remote sensing of tropospheric aerosol over land from EOS moderate resolution imaging spectroradiometer. *J. Geophys. Res.* 102: 17051–17067.

King, M.D., Kaufman, Y.J., Menzel, W.P. and Tanre, D. (1992). Remote sensing of cloud, aerosol, and water vapor properties from the Moderate Resolution Imaging Spectrometer (MODIS). *IEEE Trans. Geosci. Remote Sens.* 30: 2–27.

King, M.D., Kaufman, Y.J., Tanré, D. and Nakajima, T. (1999). Remote sensing of tropospheric aerosols from space: Past, present, and future. *Bull. Am. Meteorol. Soc.* 11: 2229–2259.

Levy, R.C., Remer, L.A., Tanré, D., Mattoo, S. and Kaufman, Y.J. (2009). Algorithm for remote sensing of tropospheric aerosol over dark targets from MODIS: Collections 005 and 051, 2nd revision, http://modisatmos.gsfc.nasa.gov/_docs/ATBD_MOD04_C005_rev2.pdf, Last Access: 2009.

Li, B., Yuan, H., Feng, N. and Tao, S. (2010). Spatial and temporal variations of aerosol optical depth in China during the period from 2003 to 2006. *Int. J. Remote Sens.* 31: 1801–1817.

Li, L.J., Ying, W.A.N.G., Zhang, Q., Tong, Y.U., Yue, Z.H.A.O. and Jun, J.I.N. (2007). Spatial distribution of aerosol pollution based on MODIS data over Beijing, China. *J. Environ. Sci.* 19: 955–960.

Li, S., Chen, L., Xiong, X., Tao, J., Su, L., Han, D. and Liu, Y. (2013). Retrieval of the haze optical thickness in North China Plain using MODIS data. *IEEE Trans. Geosci. Remote Sens.* 51: 2528–2540.

Li, W.J., Shao, L.Y. and Buseck, P.R. (2010). Haze types in Beijing and the influence of agricultural biomass burning. *Atmos. Chem. Phys.* 10: 8119–8130.

Liu, H., Tang, X.M., Cao, W., Xie, Z.Y., Lei, J.H., Li, M. and Gao, Y. (2014). Spatio-temporal variations of aerosol optical depth over areas around Beijing in recent 14 years. *Adv. Mater. Res.* 997: 843–846.

Liu, H., Gao, X.M. and Xie, Z.Y. (2015). Spatio-temporal characteristics of aerosol optical depth over Beijing-Tianjin-Hebei-Shanxi-Shandong region during 2000-2013. *Acta Sci. Circ.* 35: 1506–1511.

Liu, H.N. and Zhang, L. (2012). The climate effects of anthropogenic aerosols of different emission scenarios in China. *Chin. J. Geophys.* 55: 1867–1875 (in Chinese).

Luo, Y., Zheng, X., Zhao, T. and Chen, J. (2014). A climatology of aerosol optical depth over China from recent 10 years of MODIS remote sensing data. *Int. J. Climatol.* 34: 863–870.

Ma, Z., Liu, Y., Zhao, Q., Liu, M., Zhou, Y. and Bi, J. (2016). Satellite-derived high resolution $PM_{2.5}$ concentrations in Yangtze River Delta region of China using improved linear mixed effects model. *Atmos. Environ.* 133: 156–164.

Qi, Y., Ge, J. and Huang, J. (2013). Spatial and temporal distribution of MODIS and MISR aerosol optical depth over northern China and comparison with AERONET. *Chin. Sci. Bull.* 58: 2497–2506.

Ramanathan, V., Crutzen, P.J., Kiehl, J.T. and Rosenfeld, D. (2001). Aerosols, climate, and the hydrological cycle. *Science* 294: 2119–2124.

Remer, L.A. (2009). Executive summary, atmospheric aerosol properties and climate impacts. In *A report by the US climate change science program and the subcommittee on global change research*, Chin, M., Kahn, R.A. and Schwartz, S.E. (Eds.), National Aeronautics and Space Administration, Washington, DC, USA.

Remer, L.A., Kaufman, Y.J., Tanré, D., Mattoo, S., Chu, D.A., Martins, J.V., Li, R.R., Ichoku, C., Levy, R.C., Kleidman, R.G. and Eck, T.F., Vermote, E. and Holben, B.N. (2005). The MODIS aerosol algorithm, products, and validation. *J. Atmos. Sci.* 62: 947–973.

Salomonson, V.V., Barnes, W.L., Maymon, P.W., Montgomery, H.E. and Ostrow, H. (1989). MODIS: Advanced facility instrument for studies of the Earth as a system. *IEEE Trans. Geosci. Remote Sens.* 27: 145–153.

Smirnov, A., Holben, B.N., Eck, T.F., Dubovik, O. and Slutsker, I. (2000). Cloud-screening and quality control algorithms for the AERONET database. *Remote Sens. Environ.* 73: 337–349.

Sun, L., Sun, C., Liu, Q. and Zhong, B. (2010). Aerosol optical depth retrieval by HJ-1/CCD supported by MODIS surface reflectance data. *Sci. China Earth Sci.* 53: 74–80.

Sun, L., Wei, J., Bilal, M., Tian, X., Jia, C., Guo, Y. and Mi, X. (2015). Aerosol optical depth retrieval over Bright areas using landsat 8 OLI images. *Remote Sens.* 8: 23.

Sun, L., Yu, H., Fu, Q., Wang, J., Tian, X. and Mi, X. (2016). Aerosol optical depth retrieval and atmospheric correction application for GF-1 PMS supported by land surface reflectance data. *J. Remote Sens.* 20: 216–228.

Twomey, S. and Squires, P. (1959). The influence of cloud nucleus population on the microstructure and stability of

convective clouds. *Tellus* 11: 408–411.

Van de Hulst, H.C. (1948). Scattering in a planetary atmosphere. *Astrophys. J.* 107: 220.

Vermote, E.F. and Vermeulen, A. (1999). Atmospheric correction algorithm: Spectral reflectances (MOD09). ATBD version, 4.

Vermote, E.F. and Kotchenova, S.Y. (2008). MOD09 user's Guide (J/OL), http://modis-sr.ltdri.org.

Wang, G., Cheng, S., Li, J., Lang, J., Wen, W., Yang, X. and Tian, L. (2015a). Source apportionment and seasonal variation of $PM_{2.5}$ carbonaceous aerosol in the Beijing-Tianjin-Hebei region of China. *Environ. Monit. Assess.* 187: 143.

Wang, L., Xin, J., Li, X. and Wang, Y. (2015b). The variability of biomass burning and its influence on regional aerosol properties during the wheat harvest season in North China. *Atmos. Res.* 157: 153–163.

Wei, J. and Sun, L. (2016). Comparison and evaluation of different MODIS aerosol optical depth products over the Beijing-Tianjin–Hebei region in China. *IEEE J. Sel. Top. Appl. Earth Obs. Remote Sens.* PP: 1–10.

Wu, D. (2012). Hazy weather research in China in the last decade: A review. *Acta Sci. Circ.* 32: 257–269.

Zhang, Y., Yu, H., Eck, T.F., Smirnov, A., Chin, M., Remer, L.A. and Piazzolla, S. (2012). Aerosol daytime variations over North and South America derived from multiyear AERONET measurements. *J. Geophys. Res.* 117: D05211.

Zhao, X.J., Pu, W.W., Meng, W., Ma, Z.Q., Dong, F. and He, D. (2013). $PM_{2.5}$ pollution and aerosol optical properties in fog and haze days during autumn and winter in Beijing area. *Environ. Sci.* 34: 416–423.

Zheng, J., Che, W., Zheng, Z., Chen, L. and Zhong, L. (2013). Analysis of spatial and temporal variability of PM_{10} concentrations using MODIS aerosol optical thickness in the Pearl River Delta region, China. *Aerosol Air Qual. Res.* 13: 862–876.

Zheng, Z., Chen, L., Zheng, J., Zhong, L. and Lau, A.K.H. (2011). Application of retrieved high-resolution AOD in regional PM monitoring in the Pearl River Delta and Hong Kong region. *Acta Sci. Circ.* 31: 1154.

Received for review, May 6, 2016
Revised, December 12, 2016
Accepted, December 12, 2016